

# Control of the Laser Interferometer Space Antenna

P. G. Maghami, T. T. Hyde  
NASA Goddard Space Flight Center  
Guidance, Navigation and Control Division  
Greenbelt, MD 20771

J. Kim  
Swales Aerospace, Inc.  
Greenbelt, MD 20771

## ABSTRACT

The Laser Interferometer Space Antenna mission is a planned gravitational wave detector consisting of three spacecraft in heliocentric orbit. Laser interferometry is used to measure distance fluctuations between test masses aboard each spacecraft to the picometer level over a 5 million kilometer separation. The Disturbance Reduction System comprises the pointing and positioning control of the spacecraft, electrostatic suspension control of the test masses, and point-ahead and acquisition control. This paper presents a control architecture and design for the Disturbance Reduction System to meet the stringent pointing and positioning requirements. Simulations are performed to demonstrate the feasibility of the proposed architecture.

## 1. INTRODUCTION

The Laser Interferometer Space Antenna (LISA) is one of the first gravitational science missions that will detect ripples in space-time itself [1]. Gravity waves are detected by measuring the strain in space, i.e. the change in distance between a set of masses (test masses or proof masses) separated by a great distance. LISA uses laser interferometric measurement of the change in distance between test masses. The LISA mission consists of three spacecraft in heliocentric orbit. The orbits are chosen so that the three spacecraft form a roughly equilateral triangle with its center located at a radius of 1 AU and 20 degrees behind the Earth. The 5 million km arms of LISA and a very quiet acceleration environment ( $3.5 \times 10^{-15}$  m/s<sup>2</sup>/√Hz for LISA) allow for the detection of gravity wave strains to a best sensitivity of  $3 \times 10^{-24}$  strain/√Hz over the measurement band of  $10^{-4}$  to  $10^{-1}$  Hertz for a one-year observation. Stringent requirements are placed on the rotational ( $8 \times 10^{-9}$  rad/√Hz) and translational dynamics ( $10 \times 10^{-9}$  m/√Hz) of each spacecraft to ensure that the proper sensitivity for science measurements can be achieved.

The control system for LISA, called the Disturbance Reduction System (DRS), consists of five control functions:

- 1) Attitude control system (ACS): to orient the S/C to align the telescopes with incoming laser beams
- 2) Drag free control system (DFC): to maintain drag free motion of the proof masses in LISA measurement directions
- 3) Proof mass suspension control: to maintain relative attitude of the proof mass with respect to its housing and to maintain relative position of the proof mass with respect to its housing in the directions transverse to the sensitive axes
- 4) Telescope articulation control: to maintain the angle between the telescopes
- 5) Point-ahead (PA) and acquisition control: to point the outgoing beam while sensing the incoming beam

This paper builds on the previous work on the control of LISA [2,3]. It describes the design and performance of the five control functions of the LISA DRS, with particular attention given to the acquisition control. The proof mass displacement relative to its housing is measured in six degrees of freedom using capacitive sensing. This information is used to control the position of the spacecraft in translation to keep the proof mass centered in its housing and provide a drag free environment for the proof mass in the LISA measurement axes. A set of micro-Newton thrusters responds to the DFC force commands and to the ACS torque commands. The control functions are evaluated using 19 degrees-of-freedom (DOF) and 57-DOF dynamic simulation models of LISA.

## 2. ACQUISITION CONTROL

There are six links that need to be established before constellation operations can commence. The order of link acquisitions is illustrated in Figure 1. Note the arrows indicate the direction of light travel. The process starts arbitrarily with spacecraft A and establishes its incoming links (links 1 and 2). Next, an

arbitrary link between spacecraft B and C is established (link 3, here). At this point, either the link from spacecraft A to spacecraft B or the link from spacecraft A to spacecraft C needs to be established. Here, the link to spacecraft B is established first. It should be pointed out that while this link is being established its opposite link (going from spacecraft B to A) is temporarily lost since the local laser in spacecraft B has to be off. This means that spacecraft A has to maintain its attitude using the information it receives from its other detector as well as the attitude error estimates of the Kalman filter. Once link 4 is established, link 1 is re-established quickly without having to go through the full acquisition process. Links 5 and 6 are established in similar fashion. Once both links in an arm are established, both telescopes return their beam to the focused condition. This allows detection of received beam angle at the full science mode sensitivity. Biases are calibrated at each step allowing re-acquisition to be accomplished more rapidly. The star tracker bias with respect to the CCD and quad detector is continually estimated when those measurements are available. An alternative acquisition scheme involves scanning over the uncertainty cone instead of spoiling the beam in the first step.

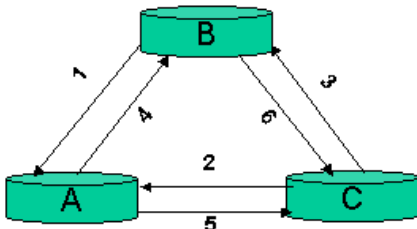


**Figure 1 LISA Acquisition Sequence**

Each spacecraft within the LISA formation receives and transmits two laser signals. The signals are used in the interferometric measurements of the LISA arms. An acquisition control is used to establish the six laser links. The strategy is sequential, in which one one-way link is established at a time. The process for the single-link acquisition is initiated from ground command and then accomplished autonomously. It is summarized as follows. (1) The gravitational sensors are first placed in accelerometer mode. (2) The two spacecraft in the link point at each other based on star tracker measurements and set their proof mass angles according to the required point-ahead angles based on orbit dynamics. A Kalman filter is designed to use the attitude error measurements from the star tracker as well as accelerometer measurements from the two GRS units to provide an enhanced estimation of the spacecraft attitude error. (3) The outgoing beam on the transmitting spacecraft is spoiled to provide a  $q$  times wider angle (but  $q^2$  times dimmer) beam that

encompasses the accuracy (noise and mounting bias) of the star tracker. (4) The other spacecraft looks for the received beam in the acquisition CCD. The CCD measurement is then used to center the received beam on the quad detector with the local laser turned temporarily off. Note: this step may be bypassed if the Kalman filter attitude error estimates provide pointing performance within the range of the detector. (5) If the beam is within the range of the detector, the received beam's centroid is measured in a direct detection quad cell mode (Direct QC), and the beam is centered within the QC. (6) The local laser is turned on, resulting in the loss of the CCD and QC signals. During the 300 seconds or so it may take to achieve phase locking and to obtain heterodyne wavefront tilt measurements, the Kalman filter estimates are used to point the spacecraft. It is expected that the pointing performance during this period would be sufficient to maintain the beam within the range of the phase meter. Once the incoming and local laser beams are locked the process moves on to the next link until all six links are phase locked and optimized.

### 3. ATTITUDE CONTROL

There are three cases considered for attitude control. These cases cover the various acquisition steps all the way to the science mode, and are discussed below.

#### Case 1: No CCD or QC Measurements

The telescope articulation is managed in an open-loop manner. The required telescope articulation angles are computed from the orbital ephemeris. Appropriate open-loop control is used to articulate the telescope properly. The articulation torque commands are fed forward to the ACS controller to decrease the disturbances on the spacecraft. An attitude error estimate is obtained from the Kalman filter. The attitude error estimates are used in the ACS control to orient the spacecraft.

#### Case 2: One-link CCD or QC Measurements

The telescope articulation is managed in an open-loop manner similar to the previous case. This case is different from the first in that CCD or QC measurements in one link are available in addition to the star tracker and accelerometer measurements. This provides enhanced attitude knowledge about two of three axes (axes normal to the telescope). An attitude error estimate is obtained from the Kalman filter. Note again that the CCD part of the process may be bypassed if the Kalman filter attitude error estimates provide pointing performance within the range of the detector. The detector measurements about the telescope Y and Z axes are augmented with the component of the attitude estimate (from the Kalman

filter) about the telescope X-axis to form the attitude error vector in the telescope frame. The attitude errors are then transformed from the telescope frame to the spacecraft frame and are used in the ACS controller to orient the spacecraft.

### Case 3: Two-link CCD or QC measurements

The ACS of each LISA spacecraft uses the incoming laser beams from the other two spacecraft to properly orient itself. Two quad detectors, one for each beam, are used to sense the direction of the incoming beam and provide a measure of attitude error to the ACS for corrective action. The ACS is designed to follow the incoming beams, and hence maintain a constant angle with the other two spacecraft. Of course, this is only possible with the in-plane articulation of one of the telescopes. Assume that two measured observation unit vectors have been computed from the quad detector measurements. The spacecraft attitude and telescope no. 1 articulation angle need to be controlled such that the two telescopes are aligned perfectly with the incoming beams (unit vectors).

First, the telescope no.1 articulation error is computed to take out the difference in the in-plane component of the first and the second incoming beams. This articulation angle error is fed to the articulation controller to properly align the in-plane angle of telescope no. 1. The spacecraft attitude error may be computed by considering the required coordinate transformation that would align the remaining components of the measured unit vectors with the desired direction vector  $\vec{o}_d$ . Assuming a telescope articulation angle of  $\beta$ , the coordinate transformation equations in the spacecraft frame may be written as follows.

$$A_e A_\beta^T A_1^T A_\beta \vec{o}_{m_1} = A_\beta^T A_1^T \vec{o}_d$$

$$A_e A_2^T \vec{o}_{m_2} = A_2^T \vec{o}_d$$

Where  $A_e$  is the unknown attitude matrix,  $A_\beta$  denotes the attitude matrix (with respect to the current telescope 1 frame) associated with the required telescope articulation,  $A_1$  denotes the current attitude matrix of the telescope 1 frame in the spacecraft frame,  $A_2$  represents the attitude matrix of the telescope 2 frame in the spacecraft frame, and  $\vec{o}_{m_1}$  and  $\vec{o}_{m_2}$  represent the unit observation vectors for telescopes 1 and 2, respectively. The attitude error may be computed from the above system of equations and is fed to the ACS controller to generate the thruster command that would properly align the spacecraft.

### **Point-Ahead Compensation**

The LISA formation is not a stationary one. In fact, because of the natural orbits of the three spacecraft, the formation plane breaths and tilts as well as the formation angles oscillates at orbital rates [4]. This means that each spacecraft is moving relative to the other two. Given that the spacecraft are roughly 5 million km apart from each other, and that the power of the 1W laser is reduced to around 70 pW at that distance, it is imperative that the each telescope points to where the other spacecraft would be in the time it takes for the light to go from one spacecraft to the other. In other words, each telescope must point ahead to where the other spacecraft will be. The point-ahead compensation is implemented in an open loop manner, wherein the telescopes are commanded at a bias to an angle defined by

$$\theta_{pa} = v_r / c$$

Where  $v_r$  represents the appropriate transverse component of relative velocity of the receiving spacecraft and  $c$  denotes the speed of light. There are two point-ahead angles for each telescope, one for each transverse direction. Meanwhile the test mass relative orientations are biased as well to an angle of  $-30\theta_{pa}$  to compensate for the prescribed point-ahead angle between incoming beam and the local.

### **4. DRAG FREE CONTROL SYSTEM**

The test masses are required to be centered within their respective housings to an accuracy of  $10 \text{ nm}/\sqrt{\text{Hz}}$ . The drag free control system is responsible for ensuring that the test masses are centered about their respective housings in the LISA measurement axes, while the electrostatic suspension control is responsible for the transverse directions. It is assumed, based on science needs, that there is no suspension control in the LISA measurement directions (optical links to the other two spacecraft). Moreover, the drag free control would arbitrarily null out the out-of-plane component of the gap error in the second test mass. This avoids the potential adverse reaction of two decentralized controllers (drag free and suspension controls) attempting to regulate on the same error.

### **5. SUSPENSION CONTROL SYSTEM**

The relative position of the two test masses in the transverse directions (except out-of-plane position of test mass no. 2) as well as the relative attitude of the test masses are maintained by the electrostatic suspension control system of the gravitational sensors. The computed relative position errors are fed to the suspension control system to produce the required electrostatic forces to null out the position errors. The

suspension controller is designed for each axis independently. However, because of the electrostatic actuation cross-talk the actual control forces and torques applied to the test masses will become coupled.

## 6. ANALYSIS RESULTS AND DISCUSSION

Preliminary designs/strategies for the five control systems of LISA have been completed. The designs have been analyzed using a 19-DOF linear model of a typical LISA spacecraft. The controller for each loop of each control system was designed independently using classical design techniques. However, the 19-DOF model, by the virtue of cross coupling between relative test mass positions, the attitude of the spacecraft, and the telescope articulation, represents a multi-input-multi-output system. Hence, the loop gains for each input and output channel (while the remaining channels are closed) were analyzed for proper stability margins. Analyses indicate each loop to have a phase margin of at least  $40^\circ$  and a gain margin of at least 12 dB in magnitude. Both time-domain and frequency-domain analyses were performed. The root power spectral density (PSD) plots in Figures 2-7 show the contributions of the various disturbance sources. The contribution of each disturbance category represents the root sum squared (RSS) values for that category; for example, the thruster noise plot is the RSS contribution of the noise from all six thrusters. Figures 2-5 show the root PSD of the telescope pointing error. A dashed horizontal line at  $8 \text{ nrad}/\sqrt{\text{Hz}}$  defines the requirement. It is clear that the design meets the requirement and is mainly dominated by the quad detector noise and capacitive sensing noise at the low frequencies and by the thrust noise as well as sensor noise in the LISA bandwidth and higher frequencies. The designs were based on a trade-off to reduce the effect of thruster noise at lower frequencies while ensuring that the sensor noise at higher frequencies does not lead to excessive thrust command variations. Figures 6 and 7 illustrate the root PSDs of the relative positions of both proof masses with respect to their respective housings in the LISA measurement axis (along the axes of the telescopes). This required performance level is along the top of each plot at  $10 \text{ nm}/\sqrt{\text{Hz}}$ . The plots show that the system satisfies these stringent requirements, with spectra being mainly dominated by the thruster noise and capacitive sensing noise.

Time-domain analyses were also performed to investigate the performance of the acquisition strategy. Figures 8-13 show the time histories of the pointing performance of each of the six links of the LISA formation. Figures 8 and 9 illustrate the

acquisition of the two links of spacecraft A. It is observed that the two links are locked in about 800 seconds. Note that the field of view of both links stays within the range of the quad cell throughout the acquisition process, indicating that the CCD segment of the process can be bypassed. Link no. 3 (from spacecraft C to B) is established next within a few hundred seconds (see Figure 10). The last three links are established by around the 2500 sec mark. Note that in this simulation the initial time in the phase locking process for heterodyning was assumed to be 300 seconds. However, the relocking of the phase was assumed to take 100 seconds. Figures 8-13 clearly demonstrate the feasibility of the proposed acquisition process using a defocus strategy. However, issues such as background stray light, affecting the signal to noise ratio of the fine sensors, as well complexities associated with the focus mechanism will have to be addressed. Other strategies, such as a scan-based strategy as well as a thru-telescope tracker approach will be investigated in the near future.

## 7. CONCLUDING REMARKS

Preliminary architecture and designs for the LISA Disturbance Reduction System have been completed. A 19-DOF linear model of a LISA spacecraft and a 57-DOF model of the LISA have been developed and were used to analyze and validate the proposed control strategies. Both time-domain and frequency-domain analyses indicate that the LISA requirements can be met. These include establishing drag-free motion of the test masses in the science band as well as tight spacecraft attitude pointing control. Moreover, the proposed defocus strategy for LISA acquisition of its six laser links has been shown to be feasible.

## 8. REFERENCES

1. LISA: Laser Interferometer Space Antenna, System and Technology Status Report, ESA-SCI(2000)11, July 2000.
2. P. G. Maghami and T. T. Hyde, "Laser Interferometer Space Antenna Dynamics and Controls Model", *Class. Quant. Grav.* **20**, S273 (2003).
3. T. T. Hyde, P. G. Maghami, and S. M., "Pointing acquisition and performance for the laser interferometry space antenna mission", *Class. Quant. Grav.* **21**, S635 (2004).
4. S. P. Hughes, "Preliminary optimal orbit design for the Laser Interferometer Space Antenna", *Proceedings of the 25<sup>th</sup> AAS Guidance and Control Conf.*, Breckenridge CO, Feb. 2002.

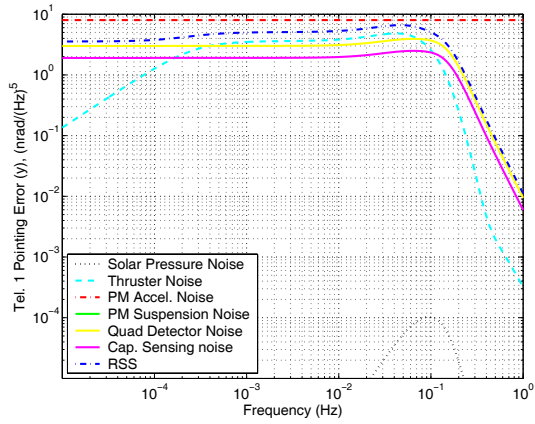


**Figure 2 Root Power Spectrum of the Pointing Error: Telescope 1, y-axis**

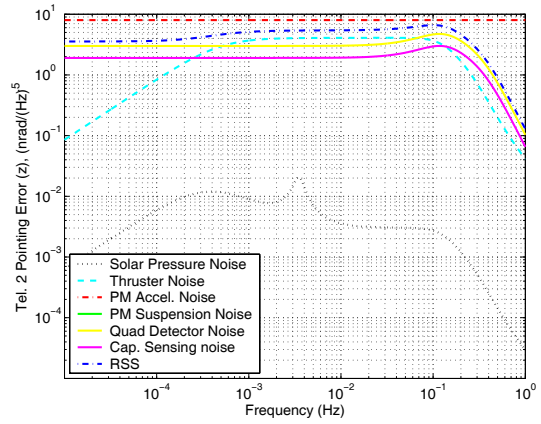


**Figure 5 Root Power Spectrum of the Pointing Error: Telescope 2, z-axis**

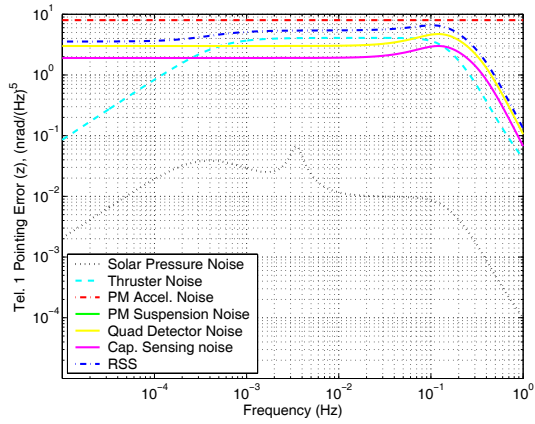


**Figure 3 Root Power Spectrum of the Pointing Error: Telescope 1, z-axis**

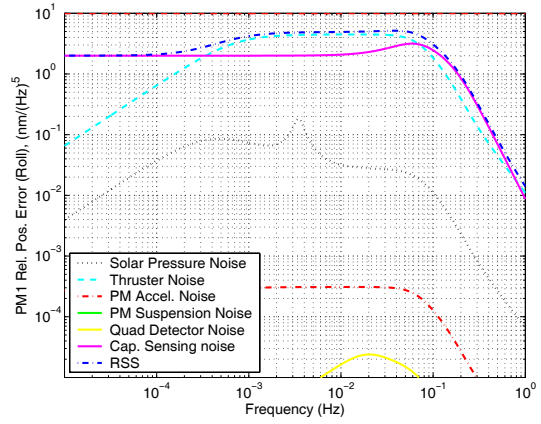


**Figure 6 Root Power Spectrum of the Relative Position of Proof Mass 1: Sensitive Axis**

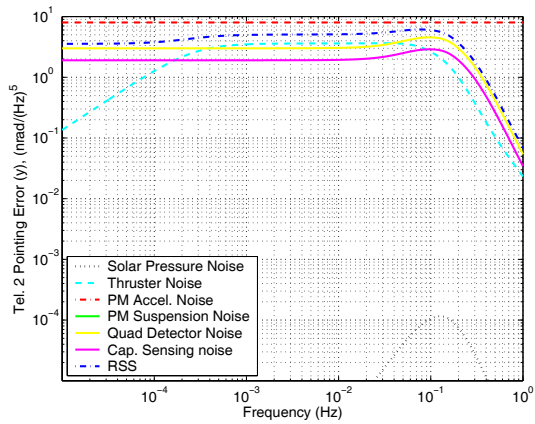


**Figure 4 Root Power Spectrum of the Pointing Error: Telescope 2, y-axis**

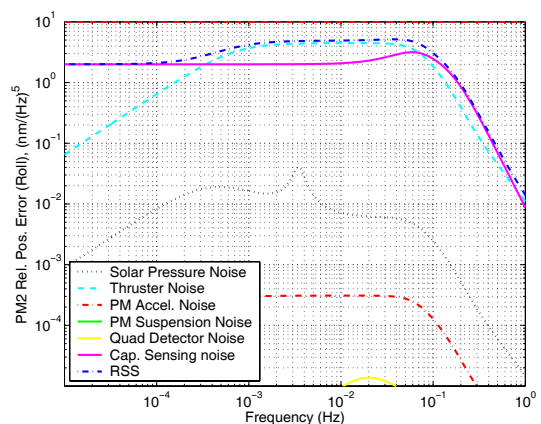


**Figure 7 Root Power Spectrum of the Relative Position of Proof Mass 2: Sensitive Axis**

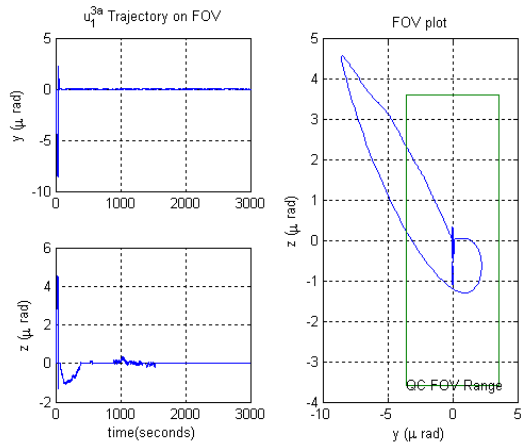


**Figure 8 Time History of Telescope Pointing Error: Link 1**

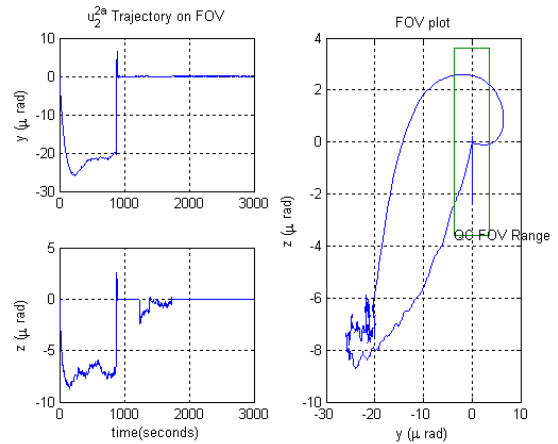


**Figure 11 Time History of Telescope Pointing Error: Link 4**

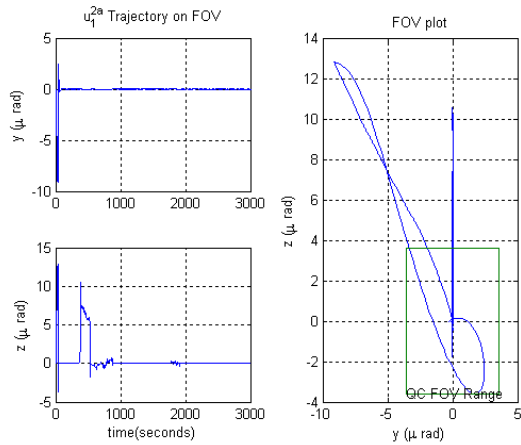


**Figure 9 Time History of Telescope Pointing Error: Link 2**

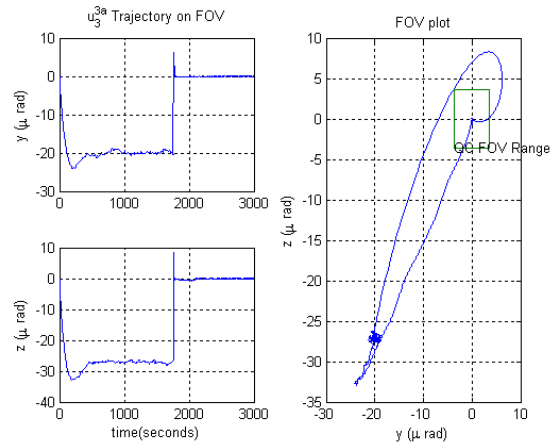


**Figure 12 Time History of Telescope Pointing Error: Link 5**

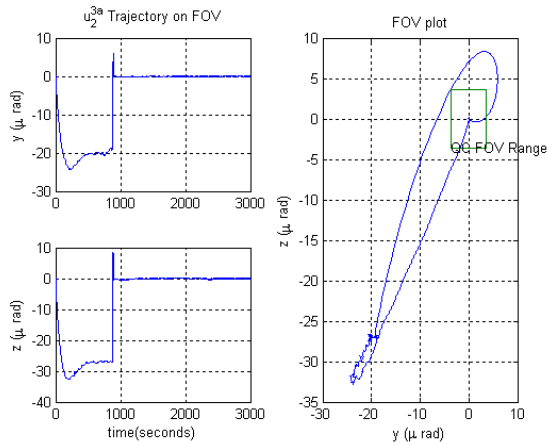


**Figure 10 Time History of Telescope Pointing Error: Link 3**

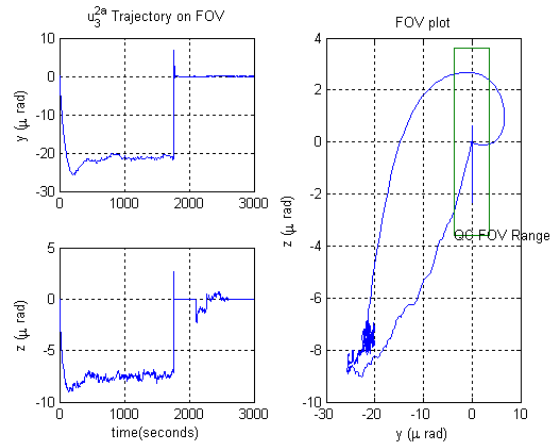


**Figure 13 Time History of Telescope Pointing Error: Link 6**